1.4 Target recoil, γ-ray and slow-neutron detectors

1.4.1 Overall design

The overall design for the recoil and γ-ray detector for EXL is divided into two major arrays, namely the EXL Silicon Particle Array (ESPA), which is assigned to detect light charged particles emerging from the target, and the EXL Gamma & Particle Array (EGPA), which covers the whole ESPA solid angle by a scintillator hodoscope and detects the punch-through charged particles as well as the gamma rays. The electronics for these two devices is essentially common. Optionally, low-energy neutrons from (p,n) reactions are detected by the EXL Low Energy Neutron Array (ELENA); this option is discussed in a separated section (see section B.1.4.6). The whole ensemble will be referred to as ERGA (EXL Recoil and Gamma Array).
The ERGA will be built over two periods. Phase I will correspond to experiments with energies close to the full capacity of the ring. In this energy domain the angular range for charged particle and gamma detection will be restricted to the more forward region in the laboratory. Phase II will be implemented for experiments with beams of energies below 40 MeV/nucleon. At these energies the solid angle coverage has to extend to 170°. Phase II will be implemented approximately two years after phase I.

The design and construction of a highly-efficient, universal recoil and gamma detector system, which will fulfil the requirements for a successful application to a wide class of reactions (see section A.2), will be one of the most challenging tasks of the present research project. In particular, the detector components need to fulfil strong demands concerning angular and energy resolutions, energy threshold, dynamic range, granularity, vacuum capability, etc., partly not available from standard detection systems. Consequently the detector design discussed in the following represents only an initial study, which needs to be reconsidered and optimised in the framework of an extensive R&D research program within the next three years.
The kinematical conditions and the resulting constraints on energy and angular resolutions are summarised in Table B.5 and Figure B.4 for a few selected typical reactions at different incident energies. Having in mind that the angular region of interest is, for direct reactions, concentrated for most cases in the c.m. angular region $0^\circ < \Theta_{cm} < 30^\circ$ (see section A.2), target-like recoil particles are to be detected in an energy interval from about 100 keV up to several hundred MeV, and in an angular region of $30^\circ < \Theta_{lab} < 120^\circ$ (except for transfer reactions, see below), which defines the constraints concerning energy threshold and dynamic range of the individual detectors. The required angular and energy resolutions to reach an overall c.m. energy resolution on the excitation energy of $\Delta E^* = 300$ keV are given in Table B.5 for individual cases.

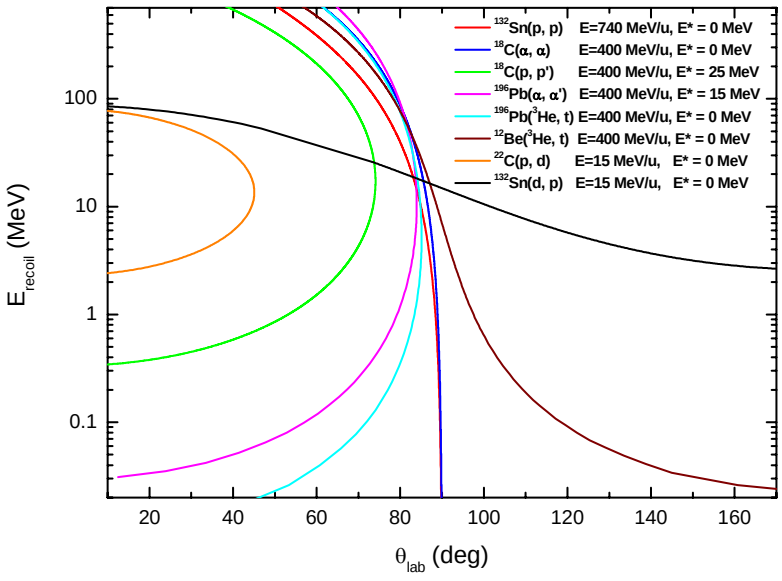

Figure B.4: *Kinematics of the target-recoil particles for selected reactions.*

A schematic view of the detector set-up surrounding the internal gas jet target (see section B.1.2) is displayed in Figure B.5. It is foreseen to separate 2 regions of the set-up with different vacuum conditions by a thin window, which could optionally be made from a thin Kapton foil. The inner "high vacuum" part will house the silicon particle array ESPA which will be bakeable to temperatures in the vicinity of 130 ºC in order to reach a vacuum of at least 10^{-7} – 10^{-8} mbar. For such a scenario a differential pumping scheme is requested with apertures of approximately 1 cm diameter at the entrance and exit of the scattering chamber, thus limiting the gas load of the NESR beam lines (see section B.1.2). For the highest target densities of up to ≥ 10^{14} / cm^2 of the H, D, ^{3}He, ^{4}He, etc. gas jet targets we expect that the gas load of the target will determine the pressure in the "high vacuum" part of the scattering chamber. To avoid background from reactions of beam particles interacting with the residual gas along the beam path (mainly from elastic scattering near Θ_{lab} = 90º where cross sections up to 10^2 - 10^3 barn/sr are expected), the detector set-up will be shielded by conical tubes as indicated in Figure B.5. The outer "low vacuum" part of the detector chamber will house the scintillation detectors of the array EGPA, which is dedicated to detect the gamma-rays, as well as the residual energy of fast recoil particles, which punch through the silicon detectors. A vacuum of about 10^{-5} mbar will be sufficient for that part of the scattering chamber.

Table B.5: *Kinematics and required and expected (obtained from simulations described in section B.1.4.3) resolutions for a few selected typical reactions.*

Reaction	Energy [MeV/ nucleon] E* [MeV]	Θ_{lab} [deg]	Θ_{cm} [deg]	E_{lab} [MeV]	Resolution required for ΔE*=300 keV		Resolution expected for proposed setup		Θ_{lab} of projectile [deg]
					$\Delta\Theta_{lab}$ [mrad]	ΔE_{lab} [keV]	$\Delta\Theta_{lab}$ [mrad]	ΔE^* [keV]	
^{132}Sn(p,p)	740	89 -80	1.1 -11	0.4 -39	8.0 -0.7	360 -330	1.5	80 -550	0.01 -0.08
		80 -75	11 -17	39 -90	0.7 -0.6	330 -390	1.5 -1.2	550 -820	0.08 -0.13
	0	75 -65	17 -29	90 -260	0.6 -0.3	390 -420	1.2 -0.8	820 -1500	0.13 -0.21
^{18}C(α,α)	400	89 -80	1.6 -16	1 -87	28 -0.4	2400 -360	1.5 -2.5	150 -1200	1.6 -2.7
		80 -75	16 -24	87 -196	0.4 -0.3	360 -390	2.5 -1.5	1200 -1700	2.7 -4.0
	0	75 -65	24 -40	196 -546	0.3 -0.2	390	1.5 -0.7	1700 -2500	4.0 -6.7
^{18}C(p,p')	400	74 -55	a) 10 -3	14 -1	2.1 -9.0	100 -30	1.5	130 -220	0.53 -0.13
			b) 13 -51	21 -304	3.0 -0.5	700 -540	1.5 -0.8	260 -630	0.64 -2.3
	25	55 -30	a) 3 -1	1.1 -0.5	9.0 -26	30 -12	1.5 -1.7	220 -550	0.13 -0.05
^{196}Pb(α,α')	400	80 -75	a) 1.5 -0.9	1.2 -0.5	3.5 -4.5	60 -18	1.5	200 -270	0.03 -0.02
			b) 13 -21	91 -234	0.4 -0.2	510 -450	2.5 -1.2	1250 -2100	0.03 -0.4
	15	75 -55	a) 0.9 -0.3	0.5 -0.1	4.5 -52	18 -15	1.5 -1.6	270 -700	0.02 -0.01
			b) 21 -53	234 -1430	0.2 -0.1	450 -600	1.2 -0.5	2100 -4000	0.04 -0.9
^{196}Pb(^{3}He,t)	400	80 -75	a) 0.9 -0.6	0.3 -0.15	6.5 -10	30 -12	1.5	250 -490	0.013 -0.009
			b) 13 -21	75 -184	0.5 -0.3	450	1.3 -0.8	850 -990	0.2 -0.3
	0	75 -55	a) 0.6 -0.2	0.15 -0.03	10 -78	12 -9	1.5	490 -1200	0.009 -0.003
			b) 21 -52	184 -1080	0.3 -0.1	450	0.8 -0.5	990 -1000	0.3 -0.7
^{12}Be(^{3}He,t)	400	120 -91	0.5 -5	0.09 -5.1	0.2 -1.8	6 -150	8	1700 -270	0.1 -0.9
		89 -80	6 -18	9 -77	1.4 -0.5	210 -330	1.5 -1.3	330 -990	1.2 -3.3
	0	80 -75	18 -25	77 -156	0.5 -0.3	330 -360	1.3 -0.8	990 -1400	3.3 -4.7
		75 -55	25 - 59	156 -792	0.3 -0.2	360 -420	0.8 -0.4	1400 -3000	4.7 -10
^{22}C(p,d)	15	40 -10	a) 25 -4	6 -2.4	22 -100	430 -120	1.5	40 -60	1.6 -0.3
	0		b) 74 -156	32 -77	7 -18	980 -660	1.5 -1.3	80 -150	1.7 -3.7
^{132}Sn(d,p)	15	170 -120	3 -22	2.7 -6	150 -18	90 -160	15 -8	100 -250	0.03 -0.23
	0	120 -90	22 -45	6 -15	18 -10	160 -290	8	250 -430	0.23 -0.44

1.4.2 Detector geometry

a) EXL Silicon Particle Array (ESPA)

An overview on the detector geometry is displayed in Figure B.5 (horizontal cross section through the mid plane) and in Figure B.6, where a 3D view of the set-up from several perspectives is given.

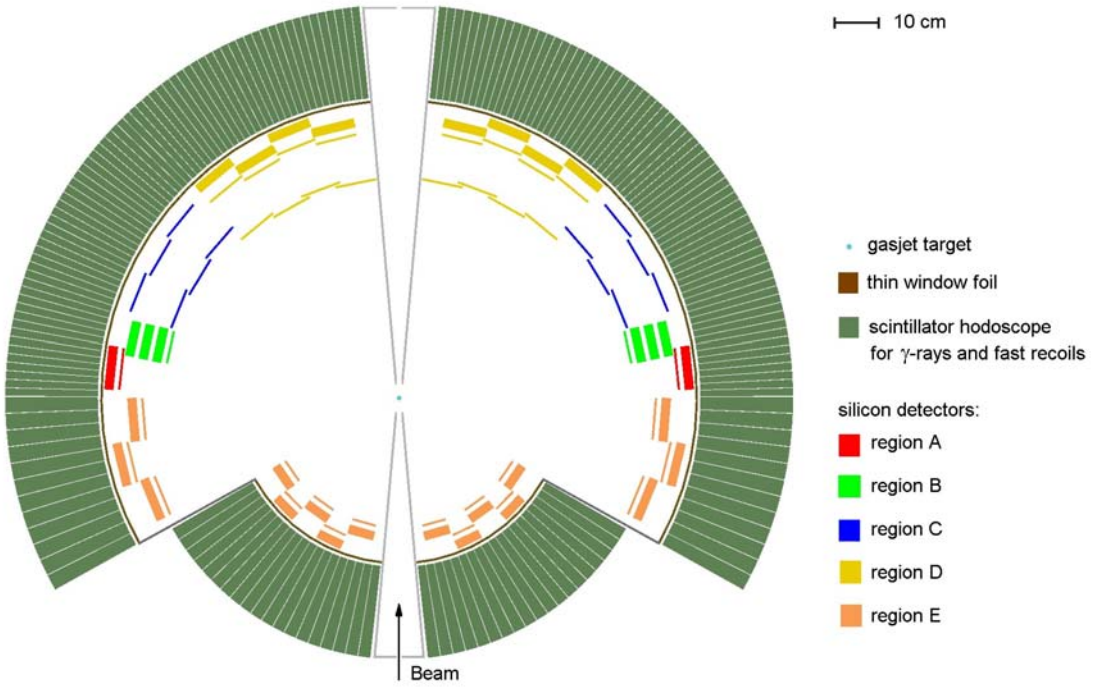

Figure B.5: *Schematic view of the detector set-up of the EXL recoil and gamma array ERGA (cross section through the mid plane)*.

In Table B.6 a list of the specifications of all individual silicon detectors is presented. Different regions A-E of the lab-angular range correspond to a colour code as defined in Figure B.5. Except for the regions C and D, where particle tracking is foreseen, the angular resolution will be determined in all other regions by the dimension of the gas-jet target and the distance of the detectors from the beam-target interaction point (sufficient position resolution of the silicon detectors assumed). Therefore a distance of 50 cm of the detectors in regions where highest angular resolution is required (see Table B.5) was chosen to obtain an angular resolution of $\Theta_{lab} \leq 2$ mrad for a target extension of 1 mm (which can be improved for certain cases by using apertures in front of the target). For measurements at larger momentum transfer performed in regions C and D, and for transfer reactions at low incident energies, which have less demanding constraints on angular resolution, a larger target extension in beam direction up to 5 -10 mm may considerably increase the luminosities.

The detectors for the angular region A are ΔE-E telescopes consisting of a double-sided silicon strip detector (DSSD), 300 μm thick, and a 9 mm thick lithium drifted silicon detector (Si(Li)) behind. Low-energy recoils from elastic scattering near 90º, as well as from charge exchange reactions with positive Q-values, will be stopped in the DSSD, whereas higher energy recoils (up to 45 MeV protons and 170 MeV α particles) will be stopped in the Si(Li). Therefore an energy threshold as low as 100 keV for the DSSD and a large dynamic range of 100 keV – 170 MeV for the combined telescope of DSSD and Si(Li) is required. Optionally the DSSD could be replaced in this region by a position sensitive integrated ΔE-E detectors with an ultra-thin (2 - 5 μm) ΔE detector in front (see section B.1.4.4), which would allow for a particle identification and discrimination against δ-electrons for the slow recoil particles.

In the angular domain B, recoil particles from elastic scattering, as well as from inelastic scattering (branch b in Table B.5) and charge exchange reactions, are stopped in 3 layers of Si(Li) detectors, whereas relatively slow recoil particles from inelastic scattering and from charge exchange reactions (branch a in Table B.5) are stopped in the DSSD. Consequently the DSSD are to be optimised to reach low detection thresholds.
In the angular region C, the present detection concept foresees to track high energetic recoil particles from elastic scattering and from reactions in two thin (~100μm) layers of Si and to stop them in the scintillation detectors of the gamma hodoscope located behind. Low energetic recoils from inelastic (branch a in Table B.5) and charge exchange reactions with negative Q-values are stopped in the thin Si detectors, again demanding for low detection thresholds. The thin Si detectors can consist of DSSD or MAPS (see section B.1.4.4).
Angular regions D and E are foreseen for the investigation of transfer reactions (pickup reactions in the forward angular range $10^\circ < \Theta_{lab} < 40^\circ$, and stripping reactions in the backward angular range $75^\circ < \Theta_{lab} < 170^\circ$) with ΔE-E telescopes consisting of DSSD and Si(Li) detectors behind. For the backward region the considerably lower constraints on angular resolution allows to place the detectors closer to the target. In addition, part of the detectors in the angular regions $45^\circ < \Theta_{lab} < 30^\circ$ and $120^\circ < \Theta_{lab} < 90^\circ$ are used for the investigation of inelastic and charge exchange reactions at c.m. angles close to 0º (see Table B.5). A first layer of tracking detectors, foreseen in the forward angular region, will allow for the investigation of quasifree scattering.

Table B.6: *Specifications of the Si detectors for the EXL silicon particle array ESPA*.

Angular region	Θ_{lab} [deg]	Detector type	Active area [mm²]	Thickness [mm]	Distance from target [cm]	Pitch [mm]	Number of detectors	Number of channels
A	89 - 80	DSSD	87 x 87	0.3	59	0.1	20	34800
		Si(Li)	87 x 87	9	60	-	20	180
B	80 - 75	DSSD	50 x 87	0.3	50	0.1	20	27400
		Si(Li)	50 x 87	9	52	-	20	180
		Si(Li)	50 x 87	9	54	-	20	180
		Si(Li)	50 x 87	9	56	-	20	180
C	75 - 45	DSSD	87 x 87	0.1	50	0.1	60	104400
		DSSD	87 x 87	0.3	60	0.1	60	34800
D	45 - 10	DSSD	87 x 87	0.1	49	0.1	60	104400
		DSSD	87 x 87	0.3	59	0.1	80	139200
		Si(Li)	87 x 87	9	60		80	720
E	170 - 120	DSSD	50 x 50	0.3	25	0.5	60	6000
		Si(Li)	50 x 50	5	26	-	60	240
E’	120 - 91	DSSD	87 x 87	0.3	59	0.1	60	104400
		Si(Li)	87 x 87	5	60	-	60	540
Total		DSSD					420	555400
		Si(Li)					280	2220

To optimise the detection efficiency of the recoil detector, a maximum solid angle cover allowed by the installations needed for the gas jet target is investigated. At angles close to $\Theta_{lab} = 90^\circ$ a coverage of at least $\varphi = \pm 45^\circ$ in azimuthal angle is foreseen, which can be increased in forward and backward direction. A first draft of a possible 3D detector geometry is displayed in Figure B.6. It should be pointed out that this concept is subject to further detailed investigations in the near future to define a final optimum solution.

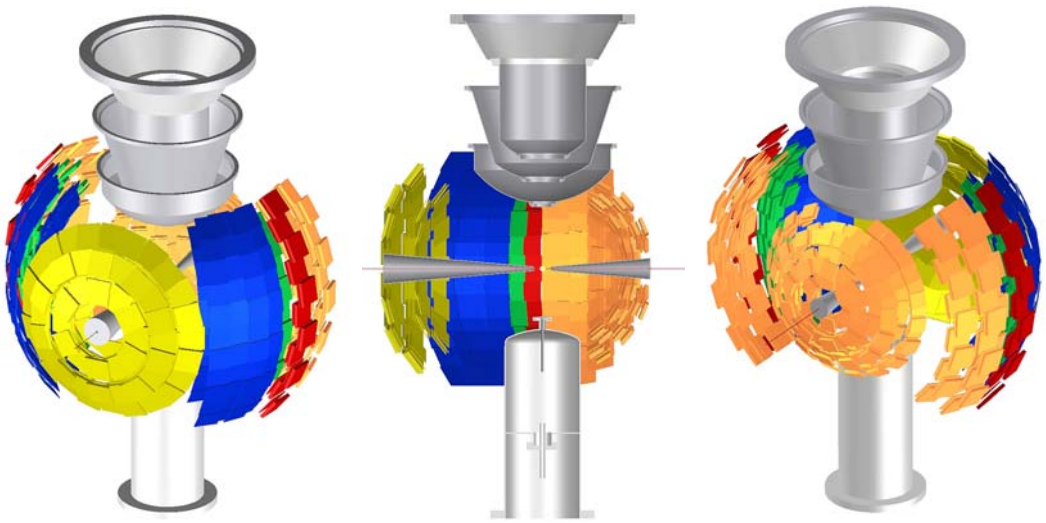

Figure B.6: *3D views of the detector arrangement of the EXL silicon particle array ESPA from several perspectives.*

Time Schedule and Milestones

2005-2006	Detector simulations. R&D on detector modules. Set-up and test of prototype detectors.
End 2006	Decision on final design. Technical design report ready.
2005-2007	Detector tests and performance studies at ESR.
Until 2009	Production of sub-units of ESPA. Installation, commissioning and test at ESR.
2009-2010	Experiments with sub-units at ESR. Production of full Phase I system.
2010	Phase I detector for NESR ready.
2010-2012	Commissioning of Phase I detector. First experiments. Production of detector modules for Phase II.
2012	Completion of ESPA for Phase II.

b) EXL Gamma and Particle Array (EGPA)

The scintillator hodoscope EGPA is supposed to detect γ-rays emitted from excited beam-like reaction products, as well as the residual kinetic energy of fast target-like reaction products, which punch through the silicon detectors of ESPA discussed above. Concerning the detection of γ-rays, aside of the γ-sum energy for missing-mass reconstruction in case the excited beam-like reaction product is particle unstable (for example after GR excitation), the detector has also to provide γ-multiplicities and individual γ-energies for spectroscopic purposes. By detecting the γ-rays from the decay of excited beam-like reaction products it also serves in separating elastic and inelastic reaction channels in cases of low-level spacing where the angular and energy resolution of the silicon detectors are not sufficient to resolve these reaction channels.

It is clear from these considerations that only a highly efficient, high-resolution device will satisfy the demands formulated above. An almost 4π coverage, sufficient detector thickness for ~ 80 % γ-detection efficiency at E_γ = 2 – 4 MeV and for stopping of up to 300 MeV protons, an energy and resolution of 2-3 % for γ-rays and at least 1 % for fast protons are required. In the case of γ-rays, the line broadening due to the Doppler shift, most substantial at highest beam energies, imposes a high detector granularity.
As a γ-spectrometer, which is in many aspects very similar to EGPA, needs to be designed and constructed for the R^3B project, we expect strong synergy effects, and consequently refer to section B.1.6 of the R^3B

Technical Proposal, where details on the kinematical properties, the geometrical considerations, and several scenarios with different crystal materials are presented.
The EGPA geometry is displayed in Figures B.5. and B.7. In contrast to R^3B, a coverage of the full angular range $10^o < \Theta_{lab} < 170^o$ is foreseen, since transfer reactions, which need to be investigated at relatively low incident energies where no pronounced Lorentz-boost in forward direction appears, are included in the experimental program. An effective thickness of the scintillator crystals of 20 cm, corresponding to about 10 radiation lengths for 4 MeV γ-rays, is foreseen. Several scintillator materials including cooled CsI crystals are presently under consideration, and an extended R&D program within the next 2 years is planned to find the optimum solution with respect to the required performance discussed above. From a computation of the Doppler line broadening, it appears that the angular coverage of individual crystals has to be restricted to bins in γ-ray polar emission angle of $\Delta\Theta_{lab} = 1 - 4^o$, depending on the emission angle. This will allow to achieve the required energy resolution even at highest beam energies. A preliminary design study of the geometrical 3D arrangement of the EGPA crystals is displayed in Figure B.7. The solid angle of interest is covered by a total number of about 2000 crystals configured in a dense packing with a total active volume of 0.7 m³.
In a first phase, where only investigations at high incident energies are planned (see section B.1.4.1), we intend to cover only the forward hemisphere; in phase II the set-up will include the backward hemisphere.

Time Schedule and Milestones

2005-2006	Detector simulation. R&D on detector modules. Set-up and test of prototype modules.
End 2006	Decision on final design. Technical design report ready.
2005-2007	Detector tests and performance studies.
2007-2008	Construction. Crystal production for 20% sub-units. Crystal tests.
2008-2009	Test of 20 % sub-units with external beams. Crystal production and test.
2010	Phase I detector ready.
2010-2012	Commissioning of phase I detector. First experiments. Production of detector modules for phase II.
2012	Completion of EGPA for phase II.

a)

b)

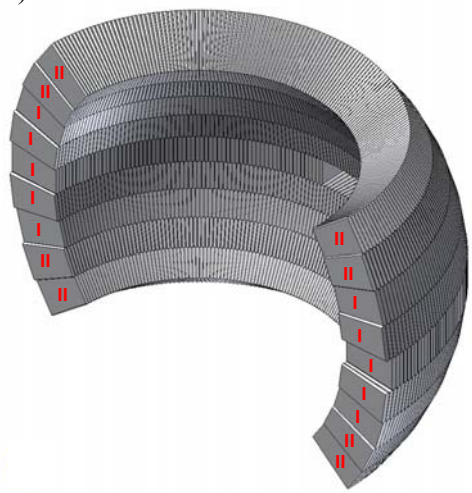

c)

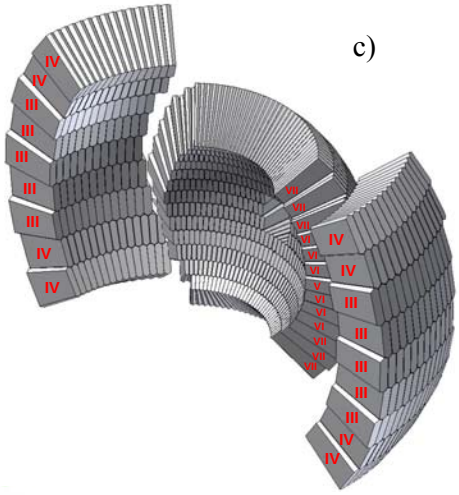

d)

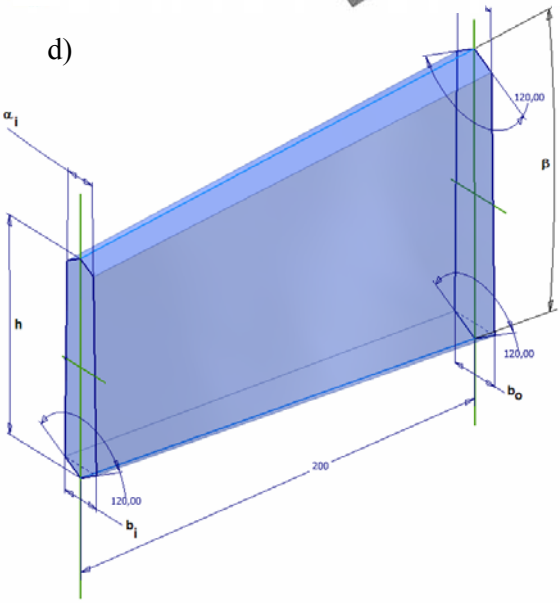

e) Configurations of CsI - crystals

Type	I	II	III	IV	V	VI	VII
Φ_{lab}	10° - 90°	10°- 90°	90°- 120°	90°- 120°	120°- 170°	120°- 170°	120°- 170°
α_i	0°	0,9°	0°	1,2°	0°	1,2°	1,8°
b_i	13,0	12,0	26,5	24,0	17,0	17,0	13,5
h	100	100	100	100	50	50	50
β	8,8°	8,8°	8,8°	8,8°	7,8°	7,8°	7,8°
α_o	0°	0,9°	0°	1,4°	0°	1,4°	1,8°
b_o	17,0	15,5	35,7	31,0	27,0	27,0	21
n	718	586	124	116	36	234	216

Figure B.7: *Design study for the geometrical arrangement of the EGPA detector: a) full setup, b) forward region (10° < Θ_{Lab} < 90°) covered by 1304 single crystals of type I and II, c) backward region (90° < Θ_{Lab} < 170°) covered by 726 single crystals of type III – VII, d) geometry of the single crystals, e) parameter list of single crystals of type I – VII.*

1.4.3 Simulations on the performance of the detection system

As already discussed above, the main requirements are high resolutions for momentum and energy of the recoiling target nuclei and a low detection threshold. Detailed simulation studies of the performance of the suggested detector scheme will show its feasibility. Some initial simulations have already been carried out.
The simulation package is based on the general-purpose transport tool Geant4 [Ago03]. It is able to trace particles through various layers of material, generate secondary particles according to the interaction cross sections and the decay probabilities of the incident particles, as well as to calculate their energy loss and time-of-flight. The analysis of the simulated events is done using the histogram tool ROOT [Bru97]. The recoil particles are generated using external event generators. The main results of the simulations carried out so far have been obtained for one of the most demanding type of reaction, namely inelastic scattering.

The aim of the simulation is to find the conditions which optimise the detection system in terms of its tracking capability and detection with good energy and angular resolution and particle identification. In particular the focus is on the following points:

- tracking section – distance from the target to the first Si micro-strip layer, distance between the layers, thickness of the 1st layer, strip pitch, thickness of the 2nd layer, strip pitch
- non-tracking section – distance from the target to the detector, thickness of the layer, strip pitch
- thickness and material of the vacuum chamber wall
- thickness and material of the scintillator hodoscope
- energy resolution for combination of several detectors

The most important parameters of the detector system are resolutions on excitation energy and on centre-of-mass scattering angle, derived from the recoil energy and angle measured in the laboratory. These values have been calculated for the detector geometry as described in section B.1.4.2. To demonstrate the influence of the thickness of the first tracking detector this parameter was varied from 30 to 100 μm. As for the quality of the stored beam and the intrinsic detector resolutions the following assumptions (based on known test results) were made:

- beam diameter: 1 mm;
- energy resolution of the silicon detectors: 50 keV (FWHM)
- energy resolution of the scintillation detectors: 1 % (FWHM)

Within the simulations performed all extracted parameters are folded with the respective resolutions. The coordinate determination is based on the strip width in the micro-strip detectors. The resolution on excitation energy ΔE^* (σ) versus proton recoil energy E_p for the case of inelastic scattering of $^{12}C(p,p')$ with E = 400 MeV/nucleon is shown on the left-hand panel of Figure B.8. The resolution on the centre-of-mass angle $\Delta\theta$ (σ) versus E_p for the same reaction is shown in the right-hand panel of Figure B.8. The results of the simulations for the higher energy (E = 740 MeV/nucleon) and heavier ions (^{132}Sn, ^{187}Pb) are plotted in Figures B.9 and B.10.

Different detector arrangements are adopted:

- two layers of strip detectors (tracking section) choosing thicknesses varying from 30 to 100 μm, relevant for the detection of particles of higher energy, e.g., protons above ~ 50 MeV, and
- only one layer of strip detectors (non-tracking section), relevant for the low-momentum transfer reactions such as inelastic excitation, charge exchange, or elastic scattering close to 90^o.

The following conclusions are drawn:

- The results are rather independent on the choice of the beam species and beam energy.
- The resolution in c.m. scattering ranges between 0.1^o – 0.3^o (FWHM) which is even better than the physics requirements (0.5^o binning is enough in most of the cases).
- The resolution in excitation energy amounts to a few hundred keV for low-momentum transfer according to the design goals, and to about 0.5 – 1 MeV in the high-momentum transfer regime.

Summarizing, the EXL recoil detector concept as outlined in this proposal appears to be basically capable fulfilling the physics requirement. Future simulation studies will contribute finding modifications which improve the detector performance.

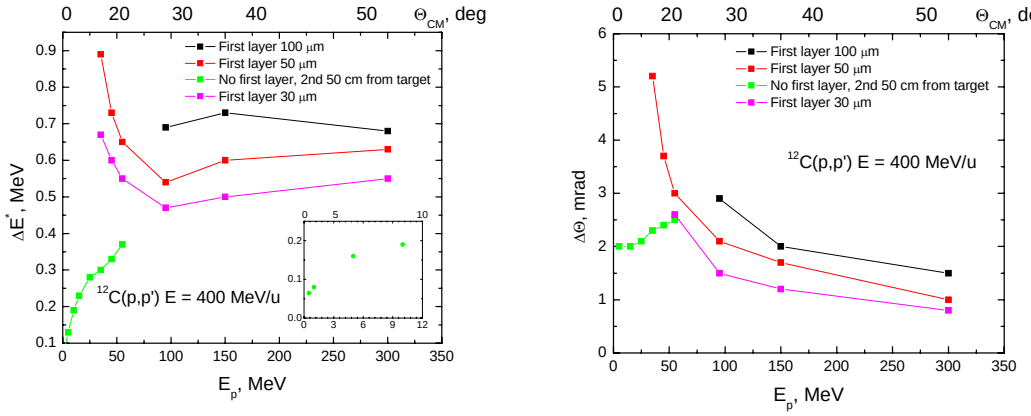

Figure B.8: *Left panel: energy resolution of the proton recoil energy E_p for the case of inelastic scattering of $^{12}C(p,p')$ with E = 400 MeV/nucleon. The inset shows the details in the region up to 12 MeV. Right panel: resolution on the centre-of-mass angle $\Delta\theta\,(\sigma)$ versus E_p for the same reaction.*

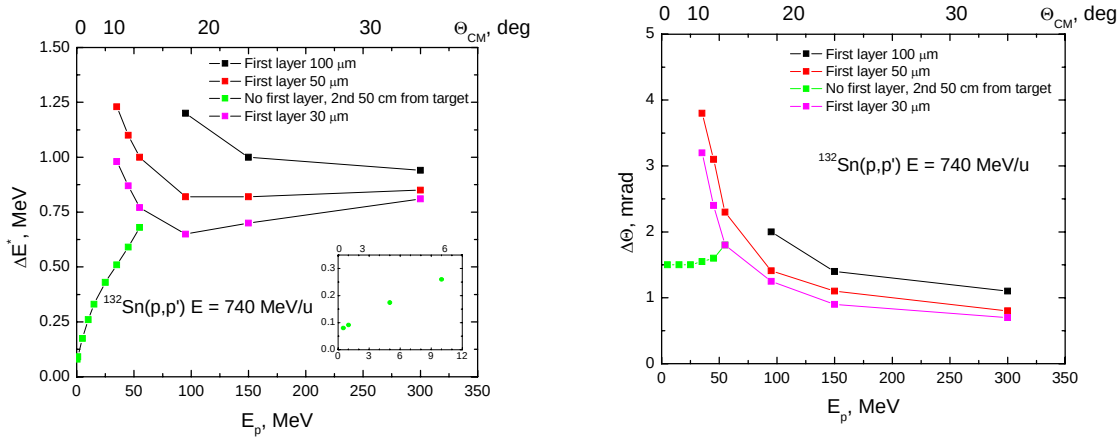

Figure B. 9: *Left panel: energy resolution of the proton recoil energy E_p for the case of inelastic scattering of $^{132}Sn(p,p')$ with E = 740 MeV/nucleon. The inset shows the details in the region up to 12 MeV. Right panel: resolution on the center-of-mass angle $\Delta\theta\,(\sigma)$ versus E_p for the same reaction.*

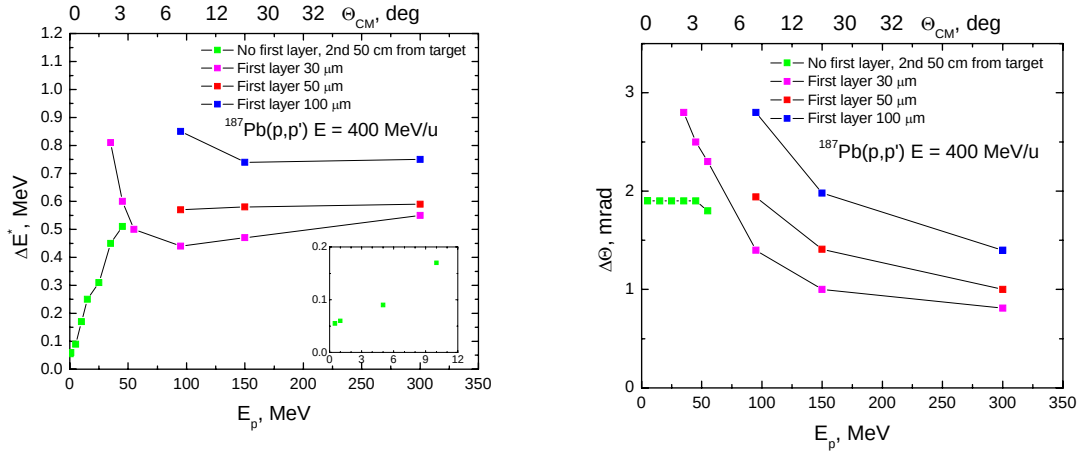

Figure B. 10: *Right panel: energy resolution of the proton recoil energy E_p for the case of inelastic scattering of $^{187}Pb(p,p')$ with E = 400 MeV/nucleon. The inset shows the details in the region up to 12 MeV. Left panel: resolution on the centre-of-mass angle $\Delta\theta\,(\sigma)$ versus E_p for the same reaction.*

Similar simulations have been performed for elastic proton and alpha scattering, inelastic alpha scattering, charge exchange and transfer reactions. Some results for the particular interesting cases are shown in Table B.5. One should mention that we assumed relatively thin (50 μm) Si detectors for the first layer of the tracking section. The obtained angular resolution $\Delta\Theta_{lab}$ is sufficient in many cases; for the (in)elastic scattering one needs to improve 2-3 times. It can be done using apertures nearby the target reducing the intersection region. The resolution on excitation energy ΔE^* is basically enough for the proton (in)elastic scattering and transfer reactions but not for some cases of alpha scattering and charge exchange reactions. The extensive R&D work and prototyping is required to reach the lowest possible detector threshold and the energy resolution of the Si and γ-ray detectors.

1.4.4 Design study

a) EXL Silicon Particle Array (ESPA)

Overview

The EXL recoil detector is Si based. Namely we present a combination of Si and Si(Li) detectors in both a classical and innovative form. It has to be said at the out-set, however, that the recoil EXL detection will be constructed for 2010 and therefore it is likely that the technology in material and detection will change before that time. We foresee that over the next two to three years there may be room for change in the choice given below. The EXL silicon recoil device will be able to detect light charged particles in a very large energy domain, ranging from a few hundreds of keV to several hundreds of MeV depending on the angle and the class of reaction in question (see Table B.5). To retain an optimal resolution with particle identification possibilities it is desirable to stop the particles in the silicon layers. However, for the higher energies, the γ-ray detector (EGPA) will have to be employed as a calorimeter for the total energy measurement.

As noted above, the Si recoil detectors covering the area around the gas-jet target need to have energy and identification over a large dynamic range (1:600). The experimental methods employed, apart from energy measurement, are (see Figure B.11):

- Time-of-flight for mass identification (TOF)
- Pulse shape discrimination for mass and charge identification (PSD)
- Standard ΔE-E
- Position resolution

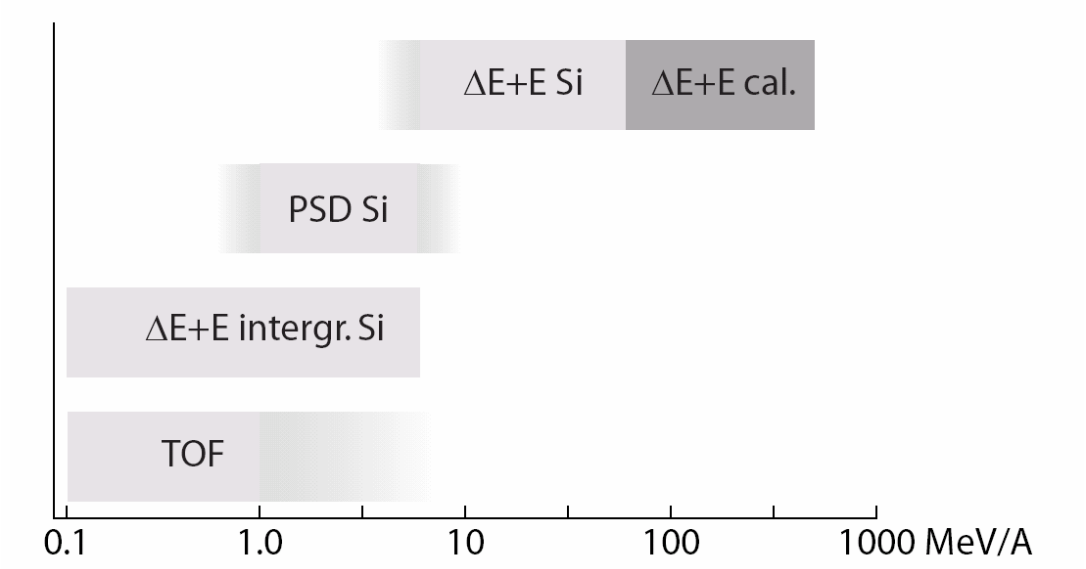

Figure B.11: *Overview of possible methods for energy measurements of light particles with identification possibilities.*

The TOF start will be delivered by the forward spectrometer once the momentum transfer/charge transfer to the quasi-projectile is sufficient to allow detection off zero degrees. Time resolutions of better than 1 ns are necessary to obtain a mass resolution better than 1/8. TOF is a standard technique; however it does depend on the existence and resolution of the start signal. Precarious and supplementary methods are therefore considered. Pulse shape analysis [Mut00] is advantageous to obtain mass and charge resolution above 1 MeV [Mut04]. To employ this method for strip detectors, R&D is required. To obtain even lower thresholds for both mass and charge resolution very thin ~1-10μm detectors are considered. Awaiting further R&D are very thin ΔE monolithic devices that combines sufficient position resolution with high active area coverage. Several methods exist to have position resolution. To allow the combined good position and low energy threshold DSSD or MAPS are retained to date.

Choice of detector types for the baseline scenario

The option retained to date for the silicon recoil device is constituted by several types of detectors. Additional options are retained for further R&D (see next section), which will enhance the physics performance of the set-up:

- **i.** 300 μm thick detectors with spatial resolution better than 500 μm in x- and y-directions. Double sided silicon strip detectors (DSSD) will be employed. The overall energy resolution required is 30 keV (FWHM).
- **ii.** Thin (≤ 100 μm) silicon detectors position sensitive in x- and y-directions. Here also DSSD, with a resolution better than 100 μm, are considered to be the principle choice. However, monolithic active pixel sensors (MAPS) are retained as an alternative. The overall energy resolution required is 30 keV (FWHM).
- **iii.** 9 mm thick cooled Si(Li) detectors with a large area 100 x 100 mm^2. Nine pads are considered. The overall energy resolution required is 50 keV (FWHM).

The Si based recoil detector will be subject to relatively small counting rates. An upper limit is 100 kHz over the 4π cover. Therefore radiation damage effects are considered not to be of importance except at about 90° where the elastic slow scattered ions will tend to have high rates. R&D to establish the effects on the first few microns of Si will be of importance.
Cooling of the Si is of consequence. Low thresholds are required and therefore low leakage currents need to be maintained. Values of 20 pAmps/cm² are acceptable for DSSD. In addition cooling has the benefit of increasing the electron drift velocity and hence improving the time resolution.
Electron suppression and RF-induced noise within the ring can be of consequence to preserve the dynamic range. Work on this is in progress.
UHV demands on the DSSD are under study, extensive experience exist within the collaboration from in-ring experiments with CHICSi, where careful choices of materials for frames, bonding and signal lines have been made to limit out-gasing and permit baking.

R&D projects for ESPA

The detectors of types **i** and **iii** do either exist on the market or could be obtained after a moderate R&D effort from commercial manufactures. However, the remaining detectors of type **(ii)** will require R&D efforts and financial investment to obtain the requested specifications. The suitable detector technologies currently available or under development are DSSD, MAPS or ISIS (Image Sensor with In-situ Storage). The latter are described in further detail in the R^3B Technical Proposal. The R&D programs mentioned within this section will be undertaken over the next two years.

- **Thin DSSD**

DSSD constitute an established technique and several manufacturers exist; e.g. 50 μm x 105 μm pitch and 65 μm thickness have been produced for the BABAR experiment by Micron Semiconductors which could constitute a baseline option for type **ii**. However, it would be desirable to further decrease the angular straggling in the first layer by decreasing the thickness. However given that both branches of the kinematics

lines need to be reconstructed, we choose a compromise of 100 μm to allow sufficient energy loss for fast protons. The electronic noise and the performance of the detectors will allow a final value to be established.
To conform with the very low energy thresholds a very small dead volume at the entrance window is requested. New techniques exist and are available on the market to reduce the dead volume to a total of 0.2 μm. To profit from such capabilities electronic front-ends are foreseen.
DSSD will be housed in the UHV and therefore the construction of such detectors (frames, glue, connectors etc.) has to fit these specifications. Baking to temperatures of 130°C is necessary.
The low energy threshold and good energy resolution is of consequence particularly for the elastic and inelastic scattering physics. For the considered solutions of having DSSD or MAPS, this implies a significantly large number of channels (see below). The existing MUST II set-up shows that values of threshold better then 150 keV and resolutions (σ) below 20 keV are possible. R&D on the Si and corresponding electronics want to reach lower values when dealing with ~560,000 channels.

- **Pulse-shape discrimination with DSSD**

Pulse-shape discrimination (PSD) has been shown to work well in order to identify intermediate mass fragments down to an equivalent range of 20 μm [Mut00] (see Figure B.12). So far, an acceptable discrimination between light ejectiles like protons and α particles has been achieved down to 1 MeV [Mut04], without a special effort to lower this limit. This is still a too high threshold for the experiments in question; furthermore no attempt has yet been made to combine PSD with high position resolution in e.g. a DSSD. The technical hitches foreseen are the non-uniformity of the field due to the strip structure and non-uniformity in the resistivity in the bulk of the Si. NTD material has still to be tested for large wafers (6" wafers). Combining DSSD and PSD (types **i** & **ii**) by a sampling read-out chip is a very interesting R&D area and would in the ideal case replace all type **i** units. A positive outcome would furthermore have implications for a large range of other experiments, e.g. decay spectroscopy. The sampling electronics is discussed in the front-end electronics section (see section B1.4.5).

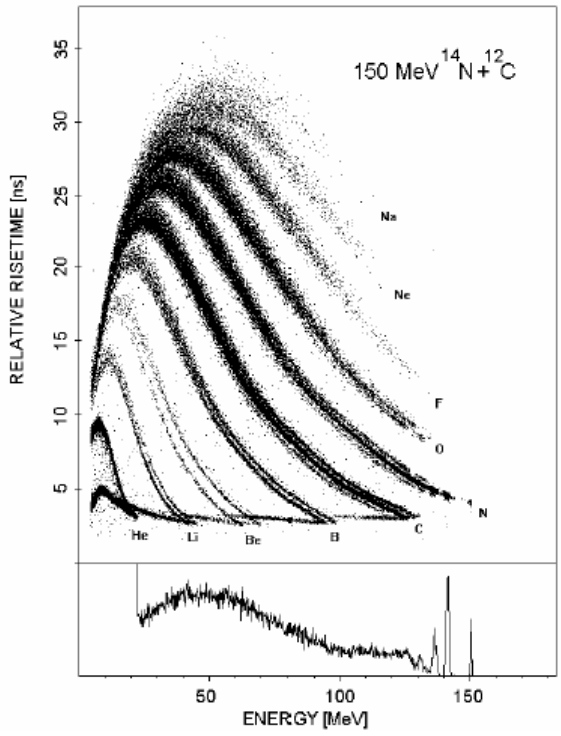

Figure B.12: *PSD plot for intermediate mass fragments, taken from [Mut00].*

- **ΔE-E MONOLITIC detectors - Integrated devices**

In recent years different techniques have been considered to develop monolithic telescopes where a very thin ΔE stage (about 1-7 μm) and a residual energy (ER) stage are integrated on the same silicon chip, e.g. [Thu97, Bor96, Car96]. In particular, monolithic telescopes having different geometries have been produced by ST-Microelectronics using high-energy ion implantation techniques, and already used to collect data in real physics experiments. All these telescopes are based on the structure sketched in the left side of Figure B.13. Basically a p^+ region is obtained via implantation on an n^- bulk. Such a p^+ region acts as a common ground electrode both for the ΔE and ER stages. In this way a ΔE active thickness of the order of 1 μm (2 μm including the dead layers) can easily be obtained.

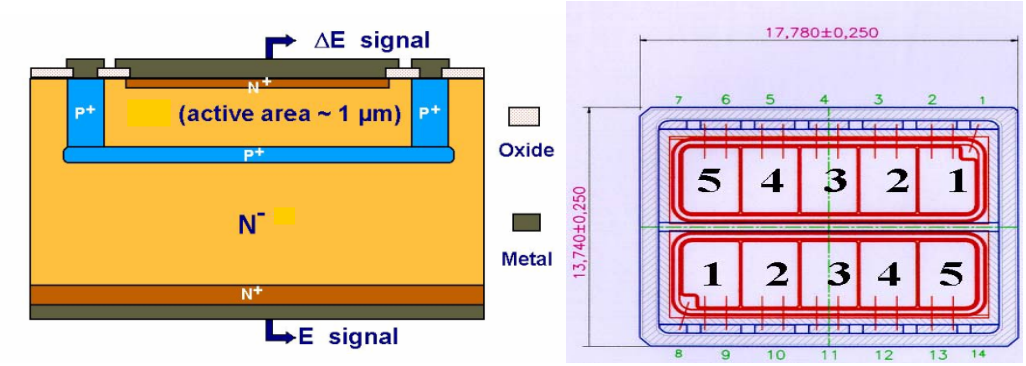

Figure B.13: *Integrated ΔE-E device.*

The first working detector had a surface of only 4x4 mm^2 [Car96]. Later, a larger area integrated telescope of 20x20 mm^2 was also developed [Tud99]. In this latter case, the large capacitance of the ΔE stage (≈40 nF) did not allow using standard preamplifiers and a dedicated prototype preamplifier was developed. Finally a detector of 15x4 mm² having 5 independent ΔE strips implanted on a common ER stage (500μm thick) has been developed [Mus98,Amo05]. This versatile detector can be used with commercial electronics since the capacitance of a single ΔE stage is of the order of 1.2 nF. For an easier handling, two of such devices were mounted on a common ceramic package to form a single detection module as sketched on the right-hand side of Figure B.13. In the tests and experiments performed a very good charge identification from Z=2 up to the heaviest detected ions (Z=25) has been obtained, with charge identification thresholds around 300-500 keV/nucleon in the charge region Z=6-25. However, the ΔE resolution is not enough to separate different isotopes of the same element [Car96, Amo05]. Due to the residual induction of the ER stage on the ΔE, the identification quality of light ions close to Z=2 may deteriorate when detectors are irradiated by heavy ions having energies of a few hundreds of MeV. Dedicated tests should be performed in this case. The β background, if present (like in radioactive ion beams induced reactions), is suppressed since the corresponding signals are going into the noise region of the ΔE due to the extremely small thickness of the ΔE stage [Amo05].

Following the positive experience with the integrated telescopes built so far, ST Microelectronics in collaboration with INFN-LNS Catania is presently working on an R&D project aiming to build a position sensitive integrated telescope having a surface of the order of 15x15 mm^2 [Amo04]. Such a detector should consist of 32 independent ΔE strips (15x0.5 mm^2 each) implanted on a common ER stage. In this detector the fired strip would provide the position information along the y-axis. At the same time, the idea is to extract the position along the x-axis from the amplitude of the signal that the ER stage induces on the ΔE strip, as discussed in [Amo04]. Although some positive results have been obtained in the first preliminary tests, further work has still to be performed to understand whether a good and reliable detector based on the above ideas can be obtained.

- **MAPS detectors**

Many current and future experiments in nuclear and particle physics need vertex detectors that are highly granular, very thin, radiation resistant, multi-layer and fast which can be installed very close to the target, or

interaction, region. Such requirements go beyond the capability of silicon-strip detectors and have prompted the development of pixel detectors. Several types of pixel detectors have been developed such as Hybrid Active Pixel Sensors (HAPS), Depleted Field Effect Transistor Sensors (DEPFETS), Monolithic Active Pixel Sensors (MAPS) and Charged Coupled Devices (CCD). Intensive R&D into developing these sensors for use as vertex detectors is underway in several laboratories, in particular in the context of the Future Linear Collider for high-energy physics and reviews of the developments can be found in [Aug04,Col03]. Of these sensor types, it appears that MAPS have some distinct advantages that also make them very promising for use as the first layer in the EXL and R^3B target recoil detectors.

The Monolithic Active Pixel Sensor is a novel silicon detector technique that integrates on the same substrate both the detector element and the processing electronics, allowing the material budget of the detector to be very low. The principle of detection is similar to that used in visible light CMOS cameras, and is illustrated in Figure B.14. Charge from a traversing particle is generated in a low-resistivity, lightly doped, p-type, epitaxial layer of 5-20 μm thickness. The electrons diffuse thermally and are collected by *n*-wells, where the signal gets converted into an electrical pulse. The *n*-wells are regularly implanted and define the pixel array. Since the lightly doped epitaxial layer is embedded between two heavily doped media, i.e. p wells and substrate, electrons reaching the boundary regions are reflected by the potential barrier due to the doping profile. This confines the charge and increases the collection efficiency. These devices benefit from the fact that a well-established process is used, which is in principle convenient to design. There are no chip connections to make and very small pixel sizes are achievable, currently down to $5\mu m^2$. This gives a position resolution of 1.5 to 3 μm. Sensors have been thinned to 10 μm and this makes the material budget very attractive, especially as there is no need for bulky chips at the edge of the detector.

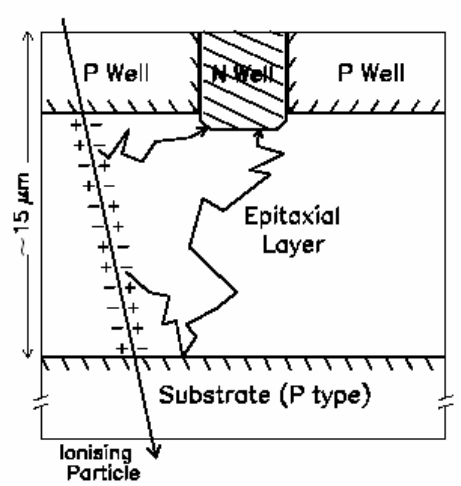

Figure B.14: *Principle of MAPS operation.*

Recent developments in the various types of pixel detectors mentioned above seem to indicate that MAPS detectors have several advantages over the other types of sensors. These advantages include :

- MAPS are made in CMOS technology, and can then take advantage of the worldwide developments in this field, in particular for the reduction of minimum feature size (MFS).
- Being monolithic, MAPS avoid the problems related to bump-bonding or other types of connections.
- Because of the shrinking size of transistors, pixels can be made very small or more functionality can be integrated in the same pixels [YanI,YanII, Kle01].
- MAPS have very low power consumption [Cho01].
- Deep submicron CMOS is radiation resistant.
- Several functionalities can be integrated on the same chip together with the sensor arrays. This brings simplification at the system level and hence reduction of costs. Pixels can be accessed randomly, trading off resolution or array size with readout speed or making it possible to track objects at very high speed [Yan01].
- The readout and analogue-to-digital conversion is always massively parallel, being normally column-parallel, but in some cases it is even pixel-parallel [YanI,YanII, Kle01].
- They can be made very easy to use, limiting the readout system requirements to digital I/Os.

Clearly many of the features of MAPS are of particular interest for the EXL and R^3B projects, where they could be used as the first layer of the target recoil detectors. Simulations have shown (see section B.1.4.3) that this first Si layer must be as thin as possible to reach the necessary precision in tracking and vertex determination and, as discussed above, MAPS detectors offer very low material budgets. Additionally, the area of the MAPS pixel can be made 100% efficient. The only inefficiency will be generated by the metal layers on top of the pixels (3 layers – 1 μm/layer; can be made thinner). For charged particles with an energy sufficiently high to penetrate the metal, the efficiency is 100%. For very low energy particles, another possibility to gain high efficiency is for the detector to be back thinned and illuminated from the back. Between detectors the dead area would be 100-200 μm. Another significant advantage is the very low power consumption of MAPS, on the order of a few tens of nW/channel. This is of crucial importance for EXL, in particular where the detectors have to be placed in ultra-high vacuum and cooling is a major issue. The possibility of an energy loss measurement in MAPS is being pursued. In principle this is possible, the noise measured in tests being 10 electrons rms. However R&D into this possibility is required.

Three man years of engineering effort is required for this R&D. Two members of the collaboration, the UK institutions and CEA-Saclay, are world leaders in the development of MAPS. Therefore, R&D can be pursued within the EXL collaboration in this direction over the next three years. Tests are foreseen to establish energy resolution and thresholds.

- **Si(Li) detectors**

As already mentioned above, EXL requires good energy measurements up to 100 MeV. Typically a sigma of 25 KeV is required. Different techniques are considered, for example Ge or CdTe, which give acceptable or even better resolution then Si(Li). However Ge is expensive and has quasi the same problems as Si(Li) with additional cryogenic difficulties. CdTe is still in its infancy when it comes to the required thicknesses and area. High-resolution scintillators, like LaBr, are also of interest however the results and their use has yet to be exercised. Thus although Si(Li) has disadvantages delimited below, it does presently have the best implementation, performance and price characteristics.
An important difficulty related to the use of semi-conductor depleted material is the loss of the active area due to the non-uniformity of the field close to the edge. The effect is known both for Si as well as for planar Ge. The loss is typically equal to the thickness of the material. This would mean that 90 cm² square detectors will have 72 cm² fully sensitive area or, for example. To maximise the active area large dimensions are required and therefore large diameter ingots. R&D is envisaged to quantify the edge effects with present techniques. Presently we consider that the frame of inactive area could be as small as 5 mm for a 9 mm thick detector slab. The maximum area that is required is typically 10x10 cm² for a number of slabs. Such an area can be cut from a 6" wafer. Up to now, production of Si(Li) detectors from 4" slices has been successful, and first investigations are underway concerning 5" material. An effort has to be made to discuss the related problems of the 5" and 6" slabs with Si crystal manufacturers. Cutting the crystal along the ingot axis is a future option.
To have a reduced capacitance and reverse current (and hence a better energy resolution) per channel each detector will be divided into approximately 10 pads. The techniques for padding Si(Li) is well understood and developed by D. Protic et al. at Jülich.

A guard-ring along the edge of the Si(Li) crystal limits the active area, but is needed for mounting purposes, to limit the noise from leakage current over the outer surface and to limit the influence of surface states:

- Usually the Si(Li) detectors are fixed by means of some clamps on a holder. The pressed contact surfaces are protected by relatively soft Indium wires or plates to prevent the damage of the contact surfaces. It is obvious that for this purpose an outer part of the detector, so called guard-ring, has to be used. At the same time the guard-ring reduces the sensitive area of the detectors. Concerning only this aspect, the guard-ring could be quite narrow, maybe 3 mm on the two opposite sides and ca. 1 mm on the others.
- A dominant part of the detector current is flowing over the outer surface between the two contacts, so called I-zone of the Si(Li) detectors. Not only the amount of this current, but also its instability causes large noise. Therefore, a guard-ring eliminates the influence of this current on the position-sensitive part of the Si(Li) detector. Also for this purpose the guard-ring could be quite narrow, ca. 1 mm.

- However, the most pronounced problem is connected with the surface states on the I-zone, which deform the electrical field near the outer surface between the contacts. According to [Lla66] the surface states induce p- or n-type channels on the I-zone. These channels distort the electrical field lines (which should be perpendicular to the contact) near the surface. For this reason, a part of the electrons or holes produced by charged particles near the surface will arrive on this surface instead of on the contacts. As the mobility of so collected charge in the surface channels is significantly reduced, the amount of the correctly collected charge will not correspond to the deposited energy of the particle. For larger thicknesses of the detector, the effect could be more pronounced. We are not sure that even a 5 mm wide guard-ring is large enough to prevent this influence of the surface states. One has to study experimentally how wide the guard-ring should be for different thicknesses. Several attempts to eliminate either the surface states or their influence on the electrical field have been made, with limited success.

During the compensation of p-type silicon by means of Li-drift, a Si(Li) detector is held under bias voltage at 100 °C. This would suggest that also a finished detector could be baked inside a scattering chamber. An important question is baking with or without an applied bias voltage:

- Baking with applied bias voltage should be a better solution, but the problem is the relatively high leakage current expected at ~100°C, which will be in the range of 1-3 mA at 500-1000 V bias.
- Without bias voltage a decompensation of the sensitive volume has to be considered. There are some indications that such a treatment could also be possible, but in any case certain investigations are needed, especially for baking at temperatures higher than 100°C.

The maximal collection times for 9 mm thick detectors will be 1800 ns at room temperature and 1000 ns at -33 °C.

- **Market survey of possible manufacturers and R&D partners for DSSD and Si(Li)**

Several manufacturers have been approached concerning developments of thin position-sensitive detectors, integrated devices and Si(Li), in addition to University laboratories:

Canberra
Canberra is clearly interested to pursue an R&D programme aimed at developing very thin DSSD as well as integrated devices after the final specifications have been defined.

Micron Semiconductors
Micron has the capability to investigate integrated ΔE-E using discrete implantations up to 100 keV in both 4" and 6"technology. Nearby, the University of Surrey also has 1 MeV implantation for deeper implants. Some ion implantation computer modelling simulations would be necessary to prepare the design. A possibility is to produce a 10 cm x 10 cm detector either single area or pixelated with a 3 to 5 μm ΔE detector integrated with a 500 μm E detector. Discrete versions of 10 μm to 20 μm ΔE single area or pixelated together with 500 μm E are possible with current technology.

ST-Microelectronic-Catania
ST Microelectronics has already developed, in collaboration with LNS–Catania, different types of integrated ΔE-E Si detectors (see e.g. [Car96,Mus98,Tud99,Amo05]) by using high-energy ion implantation techniques in 5" and 6" technology. These detectors are now commercially available. The present R&D programme [Amo04] aims to investigate the possibility to build a 15x15 mm^2 position-sensitive integrated ΔE-E device, as shortly discussed in the above summary. ST Microelectronics is generally interested in developing new types of Si detectors to satisfy the needs of different universities, laboratories or international collaborations.

Mid-Sweden University
The participating team from Uppsala University has an established contact to the clean room at Mid-Sweden University where development of integrated ΔE-E devices has been done [Thu97].

EURISYS

Over the last few years, EURISYS have invested in producing Si(Li) detectors. Using techniques as used for Ge, 2-D padding is possible. Cross-talk is acceptable. Detectors to date are made from 4" crystals. Tests with 5" are being considered.

b) EXL Gamma and Particle Array (EGPA)

Extended tests on various crystals for the exact geometry of the EGPA detectors are planned. Since CsI is the first choice of crystal, we will start with this material, where we already have performed efficiency and resolution tests on detectors of 40x40x100 mm^3 [Adv03], 20x20x15 mm^3 and 30x30x30 mm^3 volume. The optimal size of the photodiode for readout of the latter CsI detectors is 18x18 mm^2 and results given below refer to this combination when no other PD area is mentioned. The required energy resolution of about 1% for light recoils in the EXL program imposes severe constraints on the CsI(Tl)/PD properties.

The energy resolution of the CsI(Tl)/PD detector is defined (assuming a Quantum Efficiency (QE) of the PD on the level of 90%) mostly by,
i) uniformity of light collection over the active volume of CsI(Tl),
ii) efficiency of light collection
An extensive study of the CsI(Tl)/PD properties is given in [Goe04], with the aim to create a high-resolution recoil spectrometer. The tested crystal is doped with a Tl concentration of ~0.1mol%. The active size of the 18x18 mm^2 Hamamatsu S-3204-08 PD looks optimal. Tests with alpha sources and beams of protons and alphas have been performed to get the two-dimensional picture of the non-uniformity of light emission of the CsI(Tl) crystal. The light measurements reveal correlations between non-uniformity and bad resolution and it was concluded that the effect of non-uniformity comes from the non-uniform concentration of the Tl doping. Particle dependent corrections are introduced on measured light output, which finally allowed to get light output uniformity on the level of 0.1%. The following remarks comment on these results and guide towards improvements:
a) the position dependent (over the crystal front surface) light output non-uniformity looks unexpectedly high. No data are presented on absolute efficiency of light collection; our guess - less than 35% - a value that can be improved.
b) the outer area of the crystal (3 mm edges) with an effective active area 324 mm^2 /900 mm^2 (i.e. 36%) exhibits a drastic drop in the light output. This should be excluded.
c) there is a perfectly clear slope in the light output in the direction to one back facet for all tested crystal which should be investigated.

Items b) and c) may result from the geometrical structure of the CsI(Tl)/PD detector. We have made a lot of tests with the smaller CsI(Tl) crystals (20x20x15 mm^3 active volume), supplied by Khar'kov Company in Ukraine). Many different types of light guides have been tested. Two optimal lightguides are a simple one from 1 mm optical glass, which gives the same light collection efficiency as a complicated one of pyramidal type, with 20x20 mm^2 bottom facet and 10.5x11.5 mm^2 top facet. Note, that the extra rear area of CsI must be covered by 1 mm reflecting Teflon.

We used fast and quite simple pre-selection criteria regarding overall variation in light output across the face of crystal. Figure B.15 (left) shows spectra of ^{226}Ra alpha source taken with an 11 mm diameter collimator placed in the centre of the crystal of (20x20) mm^2, and with an 11 mm diameter stopping disk, placed in the centre (right). The shift in the 7.68 MeV line is only 8 channels, which means 0.27% of light output non-uniformity. This value is approximately 4 times lower than measured in [Goe04]. No visible "edge" effect was observed.

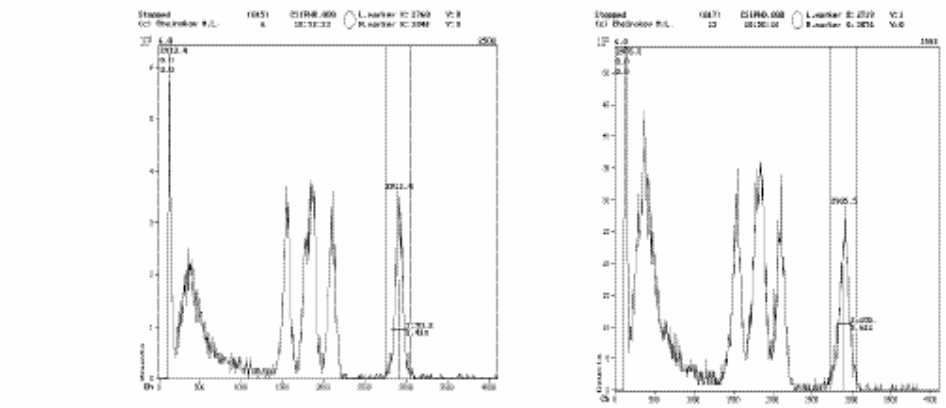

Figure B.15: *Spectra of ^{226}Ra alpha source measured by using a collimator, 11 mm diameter (left), and a 11 mm stopping disk (right). The shift of the alpha line is 0.27%.*

A detailed scan of the crystal across the face by using a 1.5 mm collimator is presented in Figure B.16. The reflecting Teflon sheet, surrounding the active area of the PD mounted in the centre of rear face of the crystal helps to get an uniform light collection. In conclusion, the light output uniformity, the absolute value of light output and the energy resolution for CsI crystal of 30x30x30 mm^3 coupled with 18x18 mm^2 PD may be obtained essentially better than that in [Goe04]. We also tested 18 smaller crystals and found energy resolution in the range of 2-3 %.

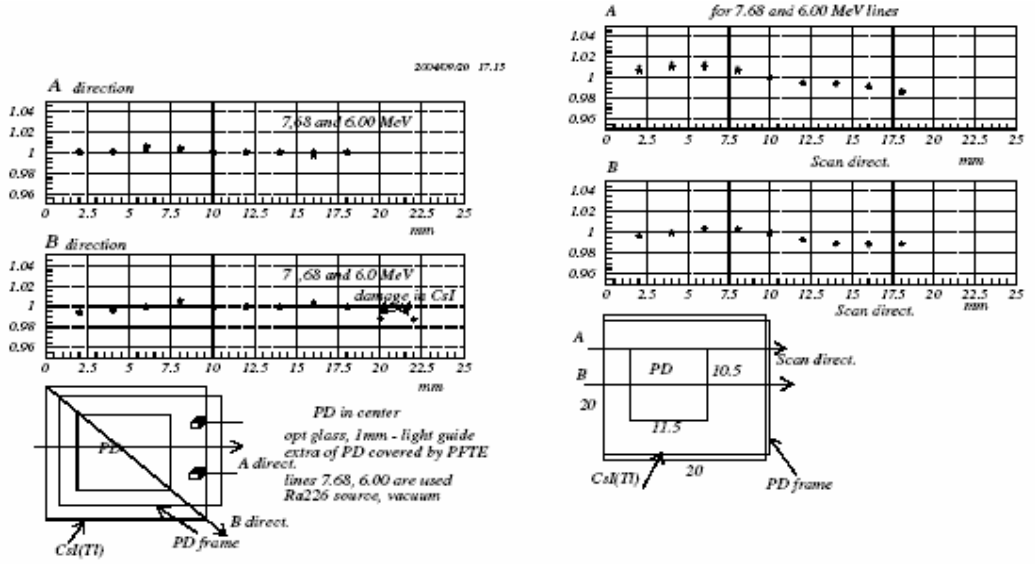

Figure B.16: *Alpha-source scan across the face of CsI by using 1.5 mm collimator.*

Figure B.17 shows the temperature variation of the light output measured for a CsI(Tl)/PMT system in the interval of T = 20 - 33^o C. The figure demonstrates the importance of temperature stabilization. The temperature gradient is dL/dT = -0.5%/1^0 C. On the other hand, the figure also shows that energy resolution can be gained by cooling of the device, e.g., to LN_2 temperature.

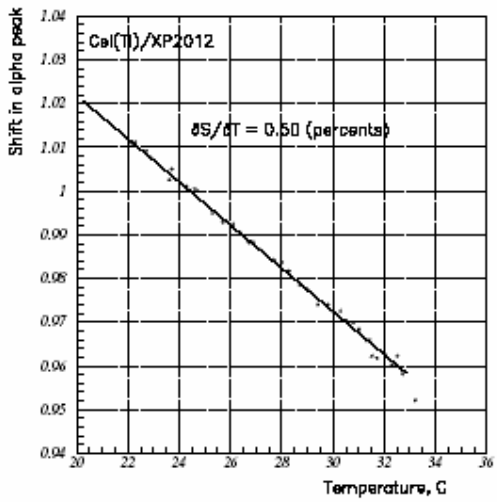

Figure B.17: *Temperature dependence of the light pulse from a CsI(Tl)/PMT detector.*

c) Vacuum chamber

The vacuum chamber is connected to the beam line via apertures and conical tubes that provide high conductance for differential pumping between the target and the storage ring, see Figure B.5. The tubes also serve as shields against events originating from background target gas. The scattering chamber has two segments separated by a Kapton foil at a radius of 620 mm. The inner vacuum chamber will have a pressure in the 10^{-7} - 10^{-8} mbar range and will be baked at least to 130º C. A baking temperature of 100°C will not be sufficient to efficiently outgas water vapour. The Si(Li) detectors which can most probably not withstand a temperature higher than 100º C will during bakeout have to be temperature stabilized by cooling. The outer chamber will have 10^{-5} mbar and will not be baked. All silicon detectors are placed in the inner chamber and the CsI calorimeter is placed in the outer chamber. As concerns the baking and installation procedure of the setup, three major steps are foreseen:

- pumping and baking the inner part including the silicon detectors,
- venting the vacuum system with a noble gas,
- installation of the CsI detectors and pumping.

It remains to be evaluated in detail if this scenario can be carried through as is, or if a more standard solution for the vacuum system is needed. In particular it needs to be investigated to which amount water vapour migration through the Kapton window will influence the vacuum conditions in the inner "high vacuum" part of the system.

The Kapton foil must be mounted so that it is not pushed inwards by the pressure difference. This can be realised by a structure with flat Kapton parts glued on to a thin metal skeleton. There are several techniques to produce the outer vacuum chamber with inwards bending windows, e.g. stainless steel and carbon-fiber reinforced epoxy. In CELSIUS there are two such parabola-shaped windows, with 550 mm outside diameter and 0.3 mm thickness, bakeable to 300 ºC, and 800 mm outside diameter with 0.4 mm thickness for the CELSIUS-WASA detector. This solution can however not easily be used for the proposed chamber since it would strongly limit the solid angle access for CsI detectors. Another possibility is a spherical outward bending structure made from aluminum or stainless steel. Such a chamber was developed for the CELSIUS cluster-jet target chamber in collaboration with CERN [Fix91] where the ANSYS code calculations are described. It has an outer diameter of 550 mm and the window is made as a semi sphere of 0.8 mm aluminum. Since it is placed symmetrically around a beam pipe there are four internal 10 x 20 mm^2 bars 90 degrees apart for reinforcement. These bars would not be necessary for a chamber without beam pipe.

Another possible geometry is a cylindrical outer chamber. This would need more CsI since the distance to these detectors would increase out of the horizontal plane. To get a strong enough window, which will have large enough safety margin against implosion it is generally needed to perform 3-dimensional calculations, e.g. with the ANSYS code. The best wall material is a duplex steel, non ferrite-austenitic, which has 3-4 times higher strength than standard 316LN material, which in its turn is superior to standard stainless steel.

For further safety it could be possible to use curved external reinforcement bars mounted vertically to minimize the loss of solid angle for CsI detectors.

As can bee seen from Figures B.5 and B.6, there is room available under the detector system for signal feedthroughs and for pumping of the chamber. Additional space for feedthroughs could possibly be fitted above the detectors close to the upper part of the cluster-jet target. To get access to the internal detector systems for mounting, cabling and service it is necessary to be able to open from at least one side. This should be possible for spherical and cylindrical geometry by using a gold wire seal.

1.4.5 Front-End Electronics

a) Overview of the design

The number of channels that need to be coded for ESPA and EGPA is approximately 560,000 and 1,500 respectively. As will be noted below the pre-amplifier section of the front-end electronics will allow for the different devices, namely DSSD, Si(Li) and PD. The objective of this section is to present a considered option for the front-end electronics, which includes the ADCs and establish the different milestones for the various parts of the required R&D.

For EXL the Si and Si(Li) detectors, together with part of the electronics, will be in UHV and the remainder in a lower vacuum. This causes difficulties associated with heat dissipation, access and feed-throughs. It is to be noted that there is a large number of channels to instrument in a comparatively small volume with a minimum of inactive volume. Thus the location of the electronics is crucial and it must be as compact as possible.

The design challenges are:

- To minimise the power per channel (substantially below 1mW, ideally 200 μW in the front end).
- To minimise the space required for electronics (hence use ASICs at the front end).
- Cover a wide dynamic range (proton energies range from 0-100 MeV and it is necessary to start to measure in the range of 100 keV).
- Good position resolution (therefore many channels).
- Accommodate both Si and Si(Li) detectors in the same ASIC.
- Electronics and detectors must survive baking (up to 130^0C).
- Electronics and detectors must not contaminate the vacuum (no out-gasing or dirt).

The parameters to be measured are**:**

- Energy.
- Position (implicit in x-y strip location).
- Time (between a discriminator and an external reference timestamp or beam pulse in the range 0-100 or 0-200 ns with sub-ns precision).
- Possibly also Pulse Shape Discrimination (PSD) (could be analogue or digital – the digital option requires an analogue pipeline to achieve fast (GHz) sampling of the leading edge to be read out with the data – this is likely to be power-hungry and consume readout bandwidth, so analogue methods will also be investigated in the search for a lower power solution).

PSD is needed for the combination of E, T where the time-of-flight/energy plot does not allow for good distinction between protons, alphas etc. The extent of the need for PSD depends on the performance achieved in the timing and energy measurement parts.

The plan is to split the ADC (which is power-hungry in an ASIC) from the remaining front-end electronics (FEE). The FEE ASIC will be in the UHV area, handling typically 32 channels and providing a multiplexed output, via a vacuum feed-through, to the ADC board which will use low power commercial ADCs. See Table B.7 for examples of today's products (remember new devices will always get faster or lower power over time.

Table B.7: *Examples from today's products.*

Company	Device	Bits	Sampling	Channels	Power/channel
Analogue Devices	AD7484	14	3MSPS	1	90mW (has sleep mode)
TI/ Burr Brown	ADS7891 ADS7890	14 14	3MSPS 1.5MSPS	1 1	90mW 60mW
Analogue Devices	AD7655	16	1MSPS	4	35mW
Linear Tech	LTC1407A	14	1.5MSPS	2	11mW
TI/ Burr Brown	ADS850	14	10MSPS	1	275mW

ASIC

The FEE ASIC will include 32 channels. We will try to fit 128 channels into each ASIC during the development phase but this cannot be guaranteed. We are confident that 32 channels can be achieved. If we manage to fit 128 channels/ASIC then we will save money compared to the above solution.

Each channel in the FEE ASIC will contain:

- Preamplifier (maybe selectable between current and charge).
- Shaping amplifier (selectable time constant 1, 3 or 4 μs, selectable gain).
- Fast (timing) amplifier for timing (selectable gain).
- Leading-edge discriminator (could perhaps be dual threshold for better timing?).
- TAC measuring from discriminator to either Timestamp clock or delayed beam pulse.
- PSD (implementation could be analogue or digital – if fast analogue pipeline then a disable will be included to reduce power when PSD is not needed).
- Multiplexer (including peak hold).
- Look-at-me logic (using discriminator output to determine whether to not participate in multiplexed readout).
- Interface to slow control (probably I2C).

The ASICs will be accommodated on a card with typically about 10 ASICs per card along with some intelligence in either a DSP or FPGA, which will be used to co-ordinate the multiplexers on the 10 ASICs into one output data stream. It will also read and write the slow control information for the ASICs to control thresholds, switch gains, switch shaping times, enable or disable the discriminator and the PSD if it is implemented with an analogue pipeline. Pulse generator with a common capacitance will be implemented. MUST II has implemented this facility. ASIC parameters will be set by group, not per channel or per ASIC. A group would comprise all the DSSD detectors in area A, another group would be the Si(Li) detectors in area A, another the DSSD in area B, etc. For detectors A-D we would need 7 groups, each with about 10 parameters to be controlled via the GUI.

ADC

The ADC cards will take data from 8 ASIC cards (320 multiplexed channels per ADC) reading at a rate between 1 and 10 MHz (limited by the settling time necessary to get 14 bit resolution). Reading all 320 channels would take 320 μs, but the look-at-me logic allows us to skip the empty channels, reading only the active channels in typically 4 or 5 μs for 4 channels. They will also have slow control (Ethernet) port (Xport or similar) and an intelligent processing/control element (FPGA or DSP) to pass the slow control information (or request for data) onto the appropriate ASIC card. Communication with the slow control system will use RPC protocol rather than explicitly issuing low-level commands via slow control. The use of Ethernet also permits the investigation of using broadcasts/multicasts to set up many channels simultaneously.

For testing and diagnostics we need to have access to each ASIC individually – this does not necessarily need to be done via the normal GUI. Each ADC card will contain enough memory to build a histogram from the channel under test (one channel per ADC card). The diagnostic software will issue RPC calls to the local intelligence in the ADC card which will initiate whatever tests are requested and return the results (or a histogram of data). Figure B.18 summarises the current EXL electronics concept.

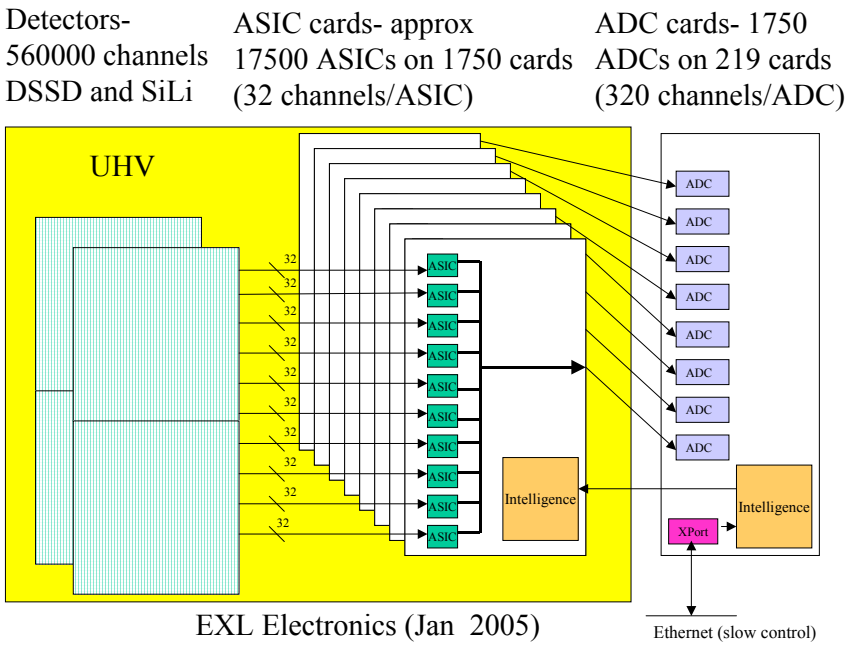

Figure B.18: *Summary of the EXL electronics.*

Power dissipation

Space projects with similar DSSD Si detectors and ASIC electronics have achieved typically 200 μW per channel for their front-end ASICs. The designs were somewhat simpler than those proposed here, but the technology is also older. Therefore 200 μW is proposed as the design aim. The channel count is 187500, so 200 μW/channel keeps the total power in the UHV from the ASICs under 40 W. The ASIC card's intelligence will need to be designed carefully – if it can be kept to 100 mW/card then the power for 600 cards is another 60 W, making a total heat load of 100 W at the front end.

Redundant cabling

It is proposed to follow the example of MUST II and to have spare (redundant) cabling between ASIC cards and ADCs which can be used under software control in the event of problems or failures.

Timestamp

The data will be time stamped with a 100 ns clock. Each ADC card will have a timestamp interface. One method of operation would be as follows: the ADC card will timestamp the data in the ASICs when it receives a Look-at-me from the ASIC (the next 100 ns clock will be sent to the ASIC card to stop its TACs and the value of the associated timestamp counter will be stored in the ADC card). If the TAC is stopped with a beam pulse then either we use the beam pulse as the timestamp clock or else we timestamp the next beam pulse using the timestamp clock after the ASIC indicates that it has data. As long as the timestamp is kept in synchronisation everywhere, there is no need for any hardware trigger – events can be selected by a software trigger later based on time, position and multiplicity criteria. (The synchronisation across hundreds of channels problem has been solved for GREAT [Laz01] and maybe other systems, so algorithms can be copied rather than developed).

Detector ID and local parameters

In MUST there is memory on the ASIC card for local detector identification and characteristic information such as leakage currents etc. It could be useful to include this information in EXL too.

Reset of shaping amplifiers in ASICs

We discussed the value of resetting the shaping amplifiers in the ASICs so that all become active together. This is a feature that is implemented but not used in MUST due to the long recovery time after resets. Problems include the case where the reset ends and the preamp is still active with the tail of an old pulse – the shaper has no "history" and so treats this like a new pulse at the input. This feature was left on the agenda for discussion but is not yet included in the ASIC specification.

Count rate and beam repetition rate

- Assume that 400 Hz is the counting rate in a single DSSD detector element (e.g. 87x87 mm^2 in angular region A, see Table B.6).
- Also assume that the rate is spread evenly over the DSSD detector.
- Assume that we see some charge sharing between strips (might not be true) – so assume each particle deposits charge in a strip and its 2 neighbours.
- Take the worst case (0.5 mm strip pitch) as an example (rate/ASIC is lower for 0.1 mm pitch).

We are planning on a 32 channel FEE ASIC, so we need 6 ASICs to instrument each face of the detector (87/0.5 = 174 channels). If the counting rate in the detector is 400 Hz, then the rate per ASIC will be 400/6 = 67 Hz (round this to 70 Hz). So, we see 3 active strips per ASIC at a rate of 70 Hz on average.

Within the ASIC we read energy and time via an analogue multiplexer, and perhaps also 100 PSD samples. So, the worst case leads to 102 mux reads per active strip = 306 mux reads for 3 active strips at a rate of 70 Hz = 21420 reads/s; round this up to 25000 reads/s. (Remember that the look-at-me mechanism skips empty multiplexer channels very quickly so we only read active channels).

The multiplexer readout rate is limited by settling time to be in the range 1 MHz to 10 MHz. For now lets assume the slowest (1 MHz). So we can perform 1000000 mux reads/s. In fact we only need, on average, 25000. So the readout is, on average 2.5% occupied which means we can still easily cope with fluctuations in the nominal 400 Hz rate.

Now, to translate this to a data rate from the whole DSSD detector (87x87 mm^2):

Each strip produces Energy (2 bytes), Time from TAC (2 bytes), PSD (200 bytes) plus a shared header word with Timestamp (6 bytes) ASIC ID (2 bytes) and hit pattern (4 bytes).

So we have 3 strip's data plus a header from each face:(3 x (2+2+200) +1x (6+2+4)) = 624 bytes and there are 2 faces giving a total 1248 bytes. At 400 Hz = 500 Kbytes/s per detector element. (20 Kbytes/s without PSD).

There are approximately 20 detector elements tiled together to cover detector region A so the data rate for all detector region A's DSSD will be 20 x 0.5 Mytes/s = 10 Mbytes/s (0.4 Mbytes/s without PSD).

The Si(Li) sees 400 Hz on only 9 contacts. Now all 9 will probably be in the same ASIC, so in this case we would need to assume that the ASIC counts at 400 Hz. If each particle produces E, T and PSD data (102 analogue values in the mux) then the mux read rate must be 41k reads/s and this is well within the 1000000 reads/s of a 1 MHz readout and allows 3 Si(Li) detectors (27 channels) to comfortably share an ASIC (total 123 k reads/s = 12.5% busy).

The data from each hit in each Si(Li) would be 204 bytes (Energy, Time + 100 PSD samples, all 2 bytes wide) and the count rate is 400 Hz. We assume no charge sharing with the large contacts, so the rate for each section of Si(Li) detectors is 82 kbytes x 20 detectors = 1.64 Mbytes/s.

Table B.8: *Summary data rate table (with PSD). The detector geometry corresponds to that defined in section B.1.4.2.*

Detector angular region	**DSSD1**	**DSSD2**	**Si(Li)**	**Total rate**
A	10 Mbytes/s		1.6 Mbytes/s	12 Mbytes/s
B	10 Mbytes/s		4.8 Mbytes/s	15 Mbytes/s
C	30 Mbytes/s	30 Mbytes/s		60 Mbytes/s
D	30 Mbytes/s	40 Mbytes/s	6.6 Mbytes/s	77 Mbytes/s
E	30 Mbytes/s		4.8 Mbytes/s	35 Mbytes/s
E'	30 Mbytes/s		4.8 Mbytes/s	35 Mbytes/s
Total				**234 Mbytes/s**

Table B.8 is calculated based on each DSSD element (regardless of size and pitch) generating 0.5 Mbytes/s of data. So 20 elements = 10 Mbytes/s, 80 = 40 Mbytes/s, etc. For Si(Li) we assume 82 kbytes/element. The detector geometry is based on that defined in Table B.6.

Synergies with DUBNA, SPIRAL II, Legnaro projects
It is important to underline the importance of this R&D. The EXL program and thus the FEE to cope with 0.5 M channels is a significant project. Therefore it can spearhead and assemble the necessary funds and manpower for a generalised front-end device for multi-channel detection systems. It should be born in mind that for this synergy to be useful the labs of interest should make an active contribution in terms of ideas and manpower.

b) Time schedule and milestones

ASIC:

Detailed ASIC specification: 12 months
ASIC development: 12 months for 1st prototype, followed by 2 periods of 9 months (4 months testing, 3 months updating design, 2 months waiting for next prototype ASIC, preparing for tests) and then 6 months to test the final prototype before committing to full wafer run.
Total= 12 months for spec and then 12 + 9 + 9 + 6 = 36 months for development (=48 months)

ASIC board:

Detailed specification: 2 months
Circuit design: 2 months
PCB design: 3 months
Wait 2 months for assembly (no manpower needed)
Test: 3 months
Rework prototype (if necessary) 2 months
Total elapsed time = 14 months

ADC board:

Detailed specification: 2 months
Circuit design: 2 months
PCB design: 3 months
Wait 2 months for assembly (no manpower needed)
Test: 3 months
Rework prototype (if necessary) 2 months
Total elapsed time = 14 months

Firmware for ADC and ASIC boards: 12 months.

Timeline:

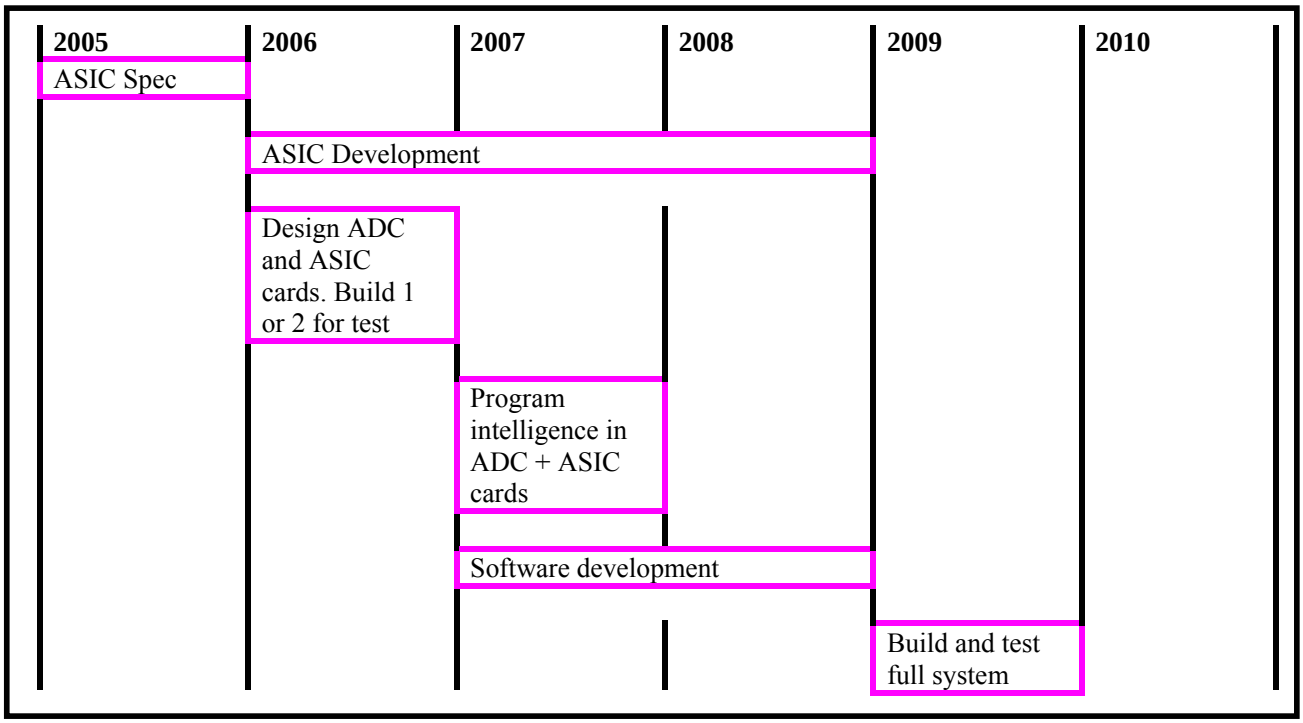

1.4.6 EXL Low-Energy Neutron Array (ELENA)

Spin-isospin giant resonances are strongly excited in (p,n) reactions. Within the EXL scheme, (p,n) charge-exchange reactions can be measured using the hydrogen gas-jet target in the NESR. We are aware, however, that in case of (p,n) reactions relatively thick targets can be used since the recoiling neutrons do not suffer from energy loss and small-angle straggling effects in the target. Experiments using external liquid or frozen hydrogen targets can thus compete in terms of resolution and luminosity achieved with the internal target. In fact, (p,n) reactions at an external target are foreseen at the R^3B experimental area, see the respective technical proposal. A detection array for low-energy neutrons (ELENA) from (p,n) reactions, nevertheless, is considered as an experimental option within the EXL concept.

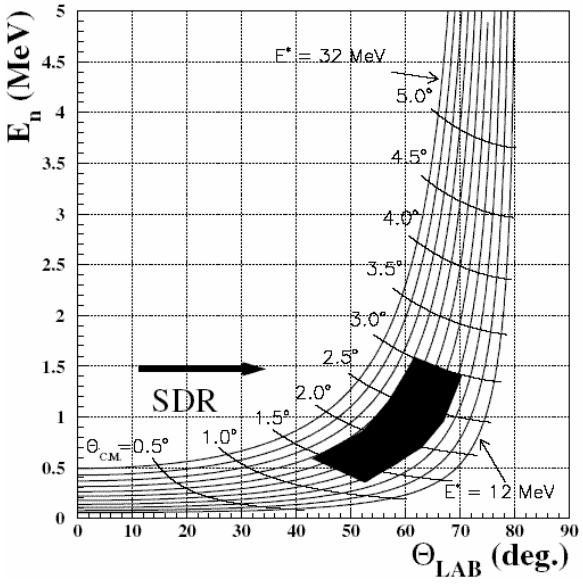

Figure B.19: *Kinematical quantities and domains for the ^{132}Sn(p,n) reaction at 400 MeV per nucleon.*

The kinematical conditions for the recoil neutrons are illustrated in Figure B.19 for the ^{132}Sn(p,n) reaction at 400 MeV per nucleon beam energy as a typical example. The kinematical domains for excitation of the isovector spin-dipole resonance (SDR) are highlighted, but the domains for other resonances, e.g., the GT resonance, are rather similar. Differential cross section for small c.m. scattering angles (1^o – 5^o) and excitation energies of 10 - 30 MeV are of interest with required resolutions of 0.5^o and 1 MeV, respectively. From the reaction kinematics, it follows that angular and energy resolutions of ~ 1^o and 10%, respectively, are needed for the neutron measurement, and laboratory angles between 50^o and 70^o have to be covered. It is envisaged to realize the detector for the low-energy neutrons from (p,n) reactions as a time-of-flight detector that covers the above range of laboratory angles. The respective part of the EXL charged-particle target detector has to be removed if (p.n) reactions are to be measured. The neutron detector will be built from organic scintillation material of 4 – 5 cm thickness, placed at 1-meter distance to the gas-jet target. The neutron detection efficiency is expected to be around 30%, the time-of-flight resolution to be about 1 ns. The main problem of such a detector arises from its detection threshold; typically 50 keV electron equivalent thresholds are achieved with conventional methods. Recent R&D, however, showed that much better results are obtained if a special wrapping (VM2000/3M) of the scintillators is used; thresholds down to 5 keV electron-equivalent energy appear within reach. This would allow detecting neutrons down to 0.5 MeV kinetic energy without significant losses in detection efficiency. A prototype detector unit with a 100 x 45 x 10 mm scintillator was already built and tested with neutrons from a ^{252}Cf source. As a next step, tests with mono-energetic neutrons produced at the cyclotron at Debrecen will be performed. The exact detector geometry will be fixed after completing the ongoing Monte-Carlo simulations. After construction, it is planned to install the device at GSI, either at the LAND setup with an external target or at the ESR internal target for bench-mark measurements prior to installation at the NESR.

Time Schedule and Milestones

Detector simulation; final design	2005
Construction	2006
Off-line test and calibration	2007
Implementation at GSI (ESR; ext. target)	2008